Since January 2020 Elsevier has created a COVID-19 resource centre with free information in English and Mandarin on the novel coronavirus COVID-19. The COVID-19 resource centre is hosted on Elsevier Connect, the company's public news and information website.

Talanta 225 (2021) 122004

Contents lists available at ScienceDirect

Talanta

journal homepage: www.elsevier.com/locate/talanta

Single-step, wash-free digital immunoassay for rapid quantitative analysis of serological antibody against SARS-CoV-2 by photonic resonator absorption microscopy

Bin Zhao [a,b,1], Congnyu Che [b,c,1], Weijing Wang [b,c,1], Nantao Li [b,d], Brian T. Cunningham [a,b,c,d,e,*]

[a] Carl R. Woese Institute for Genomic Biology, University of Illinois at Urbana–Champaign, Urbana, IL, 61801, USA
[b] Nick Holonyak, Jr. Micro and Nanotechnology Laboratory, University of Illinois at Urbana–Champaign, Urbana, IL, 61801, USA
[c] Department of Bioengineering, University of Illinois at Urbana–Champaign, Urbana, IL, 61801, USA
[d] Department of Electrical and Computer Engineering, University of Illinois at Urbana–Champaign, Urbana, IL, 61801, USA
[e] Cancer Center at Illinois, Urbana, IL, 61801, USA

ARTICLE INFO

Keywords:
Photonic resonator absorption microscopy
COVID-19 IgG
SARS-CoV-2
Active capture and digital counting
Serological diagnosis

ABSTRACT

Severe Acute Respiratory Syndrome Coronavirus 2 (SARS-CoV-2), the cause of Coronavirus Disease 2019 (COVID-19), poses extraordinary threats and complex challenges to global public health. Quantitative measurement of SARS-CoV-2 antibody titer plays an important role in understanding the patient-to-patient variability of immune response, assessing the efficacy of vaccines, and identifying donors for blood transfusion therapy. There is an urgent and ever-increasing demand for serological COVID-19 antibody tests that are highly sensitive, quantitative, rapid, simple, minimally invasive, and inexpensive. In this work, we developed a single-step, wash-free immunoassay for rapid and highly sensitive quantitative analysis of serological human IgG against SARS-CoV-2 which requires only a single droplet of serum. By simply incubating 4 μL human serum samples with antibody-functionalized gold nanoparticles, a photonic crystal optical biosensor coated with the recombinant spike protein serves as a sensing platform for the formation of sandwich immunocomplex through specific antigen–antibody interactions, upon which the detected IgG molecules can be counted with digital precision. We demonstrated a single-step 15-min assay capable of detecting as low as 100 pg mL^{-1} human COVID-19 IgG in serum samples. The calculated limit of detecting (LOD) and limit of quantification (LOQ) is 26.7 ± 7.7 and 32.0 ± 8.9 pg mL^{-1}, respectively. This work represents the first utilization of the Activate Capture + Digital Counting (AC + DC)-based immunoassay for rapid and quantitative analysis of serological COVID-19 antibody, demonstrating a route toward point-of-care testing, using a portable detection instrument. On the basis of the sandwich immunoassay principle, the biosensing platform can be extended for the multiplexed detection of antigens, additional IgGs, cytokines, and other protein biomarkers.

1. Introduction

The ongoing Coronavirus Disease 2019 (COVID-19) pandemic is caused by a novel coronavirus, now known as Severe Acute Respiratory Syndrome Coronavirus 2 (SARS-CoV-2) [1]. The rapid spread of the SARS-CoV-2 virus worldwide has led to >23.5 million documented cases and over 800 000 deaths at the time of this writing (August 2020) (https://coronavirus.jhu.edu/map.html). While detection of SARS-CoV-2 specific nucleic acid sequences by reverse transcriptase–polymerase chain reaction (RT-PCR) and (to a lesser extent) serological tests for the presence of bloodborne antigen are the predominant diagnostic assays for COVID-19 infection [2–7], these tests do not reveal the presence or intensity of a patient's immune response, or enable identification of a patient who experienced a COVID-19 infection, but was not tested while displaying a measurable viral load. Serological antibody testing is an important diagnostic tool for combating the COVID-19 pandemic [8]. Studies have shown that measurement of SARS-CoV-2 specific antibodies may be helpful for the

* Corresponding author. Carl R. Woese Institute for Genomic Biology, University of Illinois at Urbana–Champaign, Urbana, IL, 61801, USA.
E-mail address: bcunning@illinois.edu (B.T. Cunningham).
[1] B.Z., C.C. and W.W. contributed equally to this work.

https://doi.org/10.1016/j.talanta.2020.122004
Received 13 November 2020; Received in revised form 9 December 2020; Accepted 10 December 2020
Available online 14 December 2020

diagnosis of suspected patients with negative RT-PCR results and for the identification of asymptomatic infections [9]. More importantly, antibody testing can detect both recent and prior infections, while playing vital roles in epidemiology studies [10]. Measuring the immune response against SARS-CoV-2 by antibody testing is an important tool for assessing the outcomes of patients and understanding global prevalence. Quantitative assessment of SARS-CoV-2 antibody titer is especially important as clinicians and researchers more fully understand the patient-to-patient variability of immune response, in terms of the onset time for post-infection antibody production, and the post-recovery time that antibodies continue to be present [11]. As vaccines become available, it will be urgent for patients to know the extent to which their immune response has been stimulated. Furthermore, quantitative measurement of SARS-CoV-2 antibody titer in donated blood is important for blood transfusion therapy, which has shown promising results for treating patients with severe symptoms [12]. Therefore, there will be an urgent and increasing demand for serological COVID-19 antibody tests that are highly sensitive, quantitative, rapid, simple, minimally invasive, and inexpensive.

Currently, there are three methods that represent the most widely adopted serological COVID-19 antibody tests. The traditional enzyme-linked immunosorbent assay (ELISA) performed in microplates can quantify the different isotypes and subclasses of antibodies, and has been used for the detection of COVID-19 antibodies against SARS-Cov-2 spike and nucleocapsid proteins [13–15]. Chemiluminescent immunoassays (CLIA) combine the immunoassay with photon-generating chemiluminescence reporters by using a luminescent molecule-labeled antibody [16]. CLIA systems have been developed for verifying the performance of commercial COVID-19 IgG and IgM antibodies testing kits [17]. Although ELISA and CLIA offer high sensitivity and specificity, both ELSIA and CLIA-based workflows are time-consuming due to the multiple sample reagent handling and washing steps, while they also require a relatively large sample volume. The lateral flow immunoassay (LFIA) is a paper-based method that has emerged as a rapid diagnostic tool for point-of-care non-quantitative detection that offers benefits, such as low cost and ease of use [18]. However, while a number of commercial LFIAs have been rapidly developed for measuring COVID-19 IgG and IgM qualitatively [19,20], the sensitivity of LFIA is relatively low (ng mL^{-1} level) and it lacks the capability for quantitative analysis. Due to the limitations of ELISA, CLIA, and LFIA, there is an important unaddressed gap in the currently available technologies for quantitative and simple SARS-CoV-2 antibody testing. Ideally, the diagnostic workflow would require a single step, an inexpensive/portable detection instrument, an inexpensive/disposable assay cartridge, and only a fingerstick quantity of serum.

To achieve the single molecule biosensing, numerous sensing technologies have been intensely explored recently, such as electrochemical biosensors (droplet digital PCR) [21], impedance-based biosensors (nanopores) [22], interferometric biosensors (interferometric detection of scattering (iSCAT)) [23], and photonic crystal (PC)-based biosensors [24,25]. Among these digital biosensing technologies, PC-based biosensors provide a combination of low cost, simple operation, short assay time, and high sensitivity [24]. PC-based biosensors have been widely applied to the detection of multiple biological targets, such as cells, proteins, metabolites, glucose, DNAs, and RNAs [25–30]. Additionally, a diverse range of PC structures have been incorporated with other emerging technologies, such as microfluidics [31], flexible materials [32], and smartphones [33], to offer portable platforms in biosensing applications in point-of-care (POC) testing. For a recent review of digital-resolution biomolecular detection technologies, we refer the reader to Refs. [34].

In recent studies, we reported the development of a highly sensitive, single-step, enzyme-free assay with digital biomolecular precision for quantifying the presence of serum biomarkers called “Activate Capture + Digital Counting (AC + DC)” [25,31]. AC + DC uses a PC biosensor and a new form of microscopy called photonic resonator absorption microscopy (PRAM). AC + DC was initially utilized for ultrasensitive (100 aM limits of detection) detection of cancer-specific microRNA (miRNA) sequence with digital-resolution and single-mismatch discrimination without target amplification or wash steps [25], while using only a 30 μL sample volume. We further developed the AC + DC assay approach by integrating the PC biosensor into a microfluidic cartridge to demonstrate a simple quantitative viral load assay for HIV-1 p24 antigen in human serum, which required only 40 μL sample volume and provided a result in ~30 min [31].

In this work, we adapted the AC + DC assay method to demonstrate a single-step, wash–free immunoassay for rapid quantitative analysis of serological human IgG against SARS-CoV-2. Simply incubating the human COVID-19 IgG with the test sample and secondary antibody-functionalized gold nanoparticles (2^{o}Ab-AuNPs) the recombinant COVID-19 spike protein-coated PC biosensor serves as a surface for formation of sandwich immunocomplex through specific antigen–antibody interactions, enabling highly sensitive and quantitative digital-resolution detection of human IgG antibody within 15 min. Of note, the term “single-step” refers to the one-pot reaction of human COVID-19 IgG as target, 2^{o}Ab-AuNPs as detection probe and spike protein coated PC sensing platform. Without any pre-incubation step after mixing the sample and 2^{o}Ab-AuNPs in a vial, the mixture is immediately applied on the spike protein-coated PC biosensing platform for the subsequent PRAM imaging. Also, no washing steps are involved in the assay. This work represents the first utilization of the AC + DC-based immunoassay platform for rapid quantitative analysis of serological COVID-19 antibody with high sensitivity and selectivity. The calculated limit of detection (LOD) is 26.7 ± 7.7 pg mL^{-1} and the calculated dynamic detection ranges from 93.3 pg mL^{-1} to 25.7 ng mL^{-1}. The estimated limit of quantification (LOQ) is 32.0 ± 8.9 pg mL^{-1}. The results support the potential for POC testing of serological antibodies against SARS-CoV-2 using a portable detection instrument. On the basis of the sandwich immunoassay principle, this PC digital biosensing platform can be extended to become a universal analytical platform for the multiplex detection of antigens, additional IgGs, cytokines, and other protein biomarkers [35,36].

2. Material and methods

2.1. PC biosensors

The PC biosensors were fabricated on 8-inch diameter glass substrates (Moxtek, Orem, UT) based on our design specifications, and cut into 10 × 12 mm^2 pieces that were used in all experiments. The PC periodic structure, fabrication process, and resonant optical properties have been described in prior publications [25,31]. Briefly, the PC has a linear grating period of 380 nm and a grating depth of 97 nm etched into a glass substrate by reactive ion etching. The grating is coated by TiO_2 thin film with a high refractive index of 2.25 and a thickness of 98.5 nm, which yields a surface structure with high-efficiency resonant reflection at a wavelength of 625 nm when the PC surface is covered in aqueous media (Fig. S1). PCs are used once and are discarded after an assay.

2.2. PRAM instrument setup

The PC used here is a sub-wavelength periodic grating structure acting as a highly efficient narrow bandwidth resonant reflector [26,31,37]. The digital-resolution immunoassay in this work is based on the PRAM system we reported previously [25], where the light absorption of single bound plasmonic nanoparticles is dramatically enhanced when the surface plasmon-resonant wavelength of the nanoparticle matches the PC resonance wavelength. As a result, the local reflected resonant intensity from the PC is substantially reduced by the presence of individual nanoparticles (Fig. S1). Our PRAM system therefore enables the observation of single particles and digital-resolution counting of detected target molecules. A schematic diagram of the PRAM instrument used

in this work is in Fig. S2. Peak intensity value (PIV) images are obtained to visualize the captured single AuNPs under PRAM, where the value of the reflection intensity at the resonant wavelength are used as the contrast modality to provide high signal-to-noise microscopy, while using low intensity LED illumination and an ordinary uncooled image sensor. AC + DC detection is highly quantitative and robust, as it does not utilize fluorescent dyes that are subject to the effects of photobleaching.

2.3. PC silanization and functionalization

The PC surface was cleaned by acetone, isopropyl alcohol (IPA), and Milli-Q water within a series of separate glass jars and sonicated for 2 min, after which the PC was dried by N_2 and baked in an 80 °C oven for 10 min to allow the water on the PC surface evaporate. The PC surface was further cleaned and activated by a 10-min oxygen plasma treatment (Pico plasma system, diener electronic, power = 100%). Then, each PC was coated with a layer of (3-Glycidyloxypropyl) trimethoxysilane (GPTMS, Sigma Aldrich) in an 80 °C vacuum for 6 h. Redundant silane was removed by washing with toluene, methanol, and Milli-Q water sequentially. A PDMS gasket with six circular openings (diameter = 3 mm) was placed onto the PC surface to form six independent liquid compartments. For the human COVID-19 IgG capture assay, the PC was coated with 10 μL of recombinant COVID-19 spike protein (40 μg mL^{-1}, 10–011, ProSci) overnight at 4 °C. For the positive control, the PC was immobilized with 20 μL of human COVID-19 IgG (20 μg mL^{-1}, 10–551, ProSci) overnight at 4 °C. After washing with 20 μL of PBS twice, each well was filled with 20 μL of blocking buffer (SuperBlock™ in PBS, Thermo Scientific) and incubated at room temperature for 4 h to minimize the non-specific binding of AuNPs during the assay. Finally, the PC surface was washed with PBS (20 μL per well), at which point it is ready for the immunoassay.

2.4. Preparation of 2^oAb-AuNPs

2^oAb-AuNPs were prepared via EDC/NHS chemistry and heterobifunctional polyethylene glycol (PEG) linkers following the protocol we previously reported [31]. In detail, aqueous solutions of 36.5 μL of 4 μM heterobifunctional polyethylene glycol (SH-PEG-COOH, JenKem Technology), 146 μL of 1 μM 1-ethyl-3-(3-dimethylaminopropyl) carbodiimide (EDC, Thermo Scientific), 58 μL of 2.5 μM N-hydroxy succinimide (NHS, Thermo Scientific) were mixed with 174.5 μL of Milli-Q water. After pH adjustment to 7.4 by adding 50 μL of 10 × concentrated PBS and 25 μL of 0.01 M NaOH, the solution was incubated at room temperature for 1 h with gentle shaking. Then, 7 μL of 1.4 μM goat anti-Human IgG Fc highly cross-adsorbed secondary antibodies (2^oAb, A18831, Thermo Scientific) were added into the solution and incubated at room temperature for 2 h. After centrifuging at 4 °C for 10 min at 14, 000 g using a 50-kDa centrifuge filter, the mixture was further washed with PBS buffer twice under the same centrifuge conditions to remove any byproduct. The as-prepared SH-PEG-2^oAb conjugate (12 μL) was mixed with 200 μL of 80 nm diameter gold nanourchin stock solution (13 pM, Cytodiagnostics) and incubated at room temperature for 1 h with gentle shaking. After overnight incubation at 4 °C, 2 μL of SuperBlock™ blocking buffer was added to block the bare AuNP surface to eliminate non-specific binding. The 2^oAb-AuNPs were gently shaken at room temperature for 1 h and washed by centrifuge at 4 °C for 30 min at 800 g. The pellet was re-dispersed with PBS and stored at 4 °C for later use. The 2^oAb-AuNPs were characterized by a NanoDrop® ND-1000 Spectrophotometer (pathlength = 1 mm) and Dynamic Light Scattering Analyzer to confirm the conjugation of antibodies (Fig. S3).

2.5. AC + DC immunoassay for COVID-19 antibody detection

In a typical immunoassay in buffer, 9 μL of 2^oAb-AuNPs conjugate (Abs = 0.070 ± 0.005, diluted with 0.1 × PBS) was mixed with 1 μL of human COVID-19 IgG in PBS at variable concentration (0, 1, 10, 100, 1000 and 5000 ng mL^{-1}) in a 0.6 mL microcentrifuge tube. The final concentration of COVID-19 IgG is 0, 0.1, 1, 10, 100 and 500 ng mL^{-1}. For the human serum sample analysis, 6 μL of 2^oAb-AuNPs (Abs = 0.155 ± 0.005) were added into a 0.6-mL microcentrifuge tube. Serial dilutions of 100% human serum samples containing COVID-19 IgG (4 μL for each) were added to achieve a final concentration of 0.1, 1, 10, 100 and 500 ng mL^{-1}. After thoroughly mixing, the mixture was immediately added into a PDMS well attached on the spike protein-coated PC for PRAM imaging. All the assays were repeated three times independently.

2.6. Selectivity test

We selected native IgG, IgM and Human Serum Albumin (HSA) isolated from complete human serum (ab98981, ab91117, ab205808, Abcam) as control proteins. 1 μL of 100 ng mL^{-1} IgG, IgM or HSA in PBS was added to 9 μL of 2^oAb-AuNPs (Abs = 0.070 ± 0.005). For the human serum blank control (HS blank), 4 μL of complete human serum was mixed with 6 μL of 2^oAb-AuNPs (Abs = 0.155 ± 0.005). After mixing well, the mixture was immediately introduced into the PDMS well on the PC surface for PRAM imaging.

2.7. PRAM imaging

The PRAM system is built upon the body of a bright field microscope (Carl Zeiss Axio Observer Z1) (Fig. S2). A 20 × objective lens was used to acquire the resonant reflection spectrum of each pixel within the field-of-view at a line-scanning mode. A 512 × 512 pixel image was generated by collecting the reflected light using a charge-coupled device camera (Photometrics Cascade). As shown in Fig. S1, the Peak Intensity Value (PIV) represents the highest intensity of the resonantly reflected wavelength from the PC surface, and a localized reduction in PIV occurs when an AuNP attaches to the PC surface. By gathering a baseline PIV image of the PC biosensor surface before introduction of the test sample, reductions in PIV are registered by comparison of the baseline image to subsequent PIV images gathered after AuNP attachment. A watershed algorithm is applied to the resulting PIV "shift" image to identify clusters of pixels with reduced PIV, and to thus count the number of attached AuNPs in the field of view.

3. Results and discussion

3.1. Design of PRAM-based AC + DC digital immunoassay

The design of a PRAM-based AC + DC immunoassay for human COVID-19 IgG detection is schematically illustrated in Fig. 1. The immunoassay employs a typical sandwich configuration, which is based on the principle of AC + DC we previously reported [25,31]. We prepare 2^oAb-AuNPs by covalently conjugating urchin-shaped nanoparticles (nanourchins) with anti-human IgG Fc secondary antibody (Fig. 1A). The human COVID-19 IgG sample and 2^oAb-AuNPs are mixed in a tube and the mixture is immediately applied on the spike protein-coated PC biosensing platform for PRAM-based single-step immunoassay (Fig. 1B). COVID-19 IgGs will activate the system by binding either functionalized AuNPs or the spike protein-coated PC through specific antigen–antibody interaction, allowing for the subsequent capture of COVID-19 IgG-AuNP complexes or AuNPs to form sandwich immunocomplex on the PC. PRAM imaging is then conducted for quantitative detection of human COVID-19 IgG antibody by digitally counting the number of bound AuNPs on the PC (Fig. 1C), where each AuNP in the PRAM image represents one IgG target molecule. We have previously demonstrated that AC + DC–based immunoassays can effectively reduce the time requirement for a diffusion-limited assay [31]. In this work, because no pre-incubation and washing steps are required, our AC + DC immunoassay method allows for a 15-min rapid test of human COVID-19 IgG in

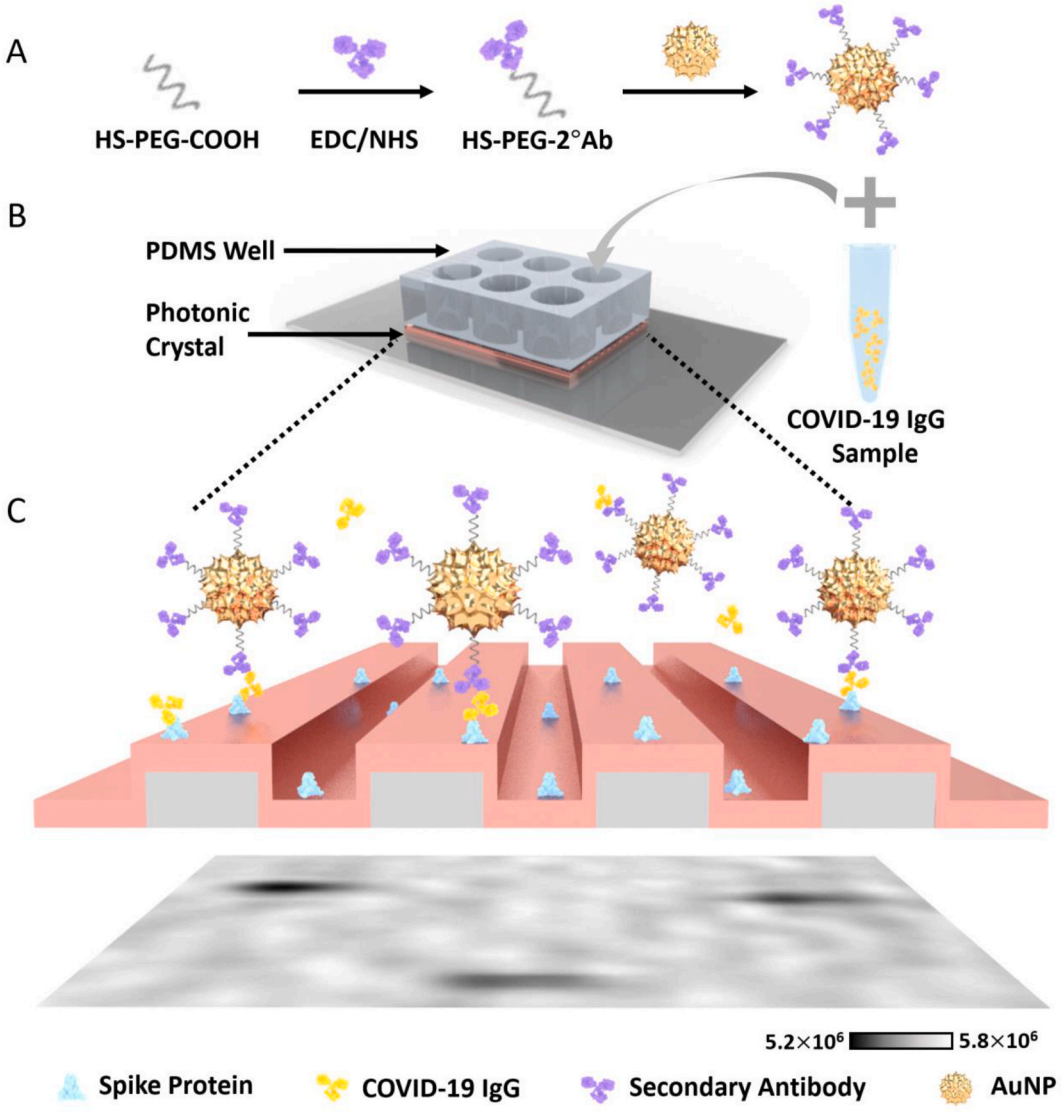

Fig. 1. Schematic illustration of PRAM-based AC + DC immunoassay for human COVID-19 IgG detection. (A) Preparation of secondary antibody (2^{o}Ab) functionalized AuNPs. Highly cross-adsorbed secondary antibodies were conjugated with 80 nm diameter gold nanourchins via EDC/NHS chemistry and heterobifunctional HS-PEG-COOH linkers. **(B)** Workflow of the PRAM-based AC + DC immunoassay. The COVID-19 IgG sample in a tube was first added to a reagent comprised of 2^{o}Ab-AuNPs and the mixture was immediately introduced into a PDMS well with spike proteins coating a photonic crystal (PC) surface, followed by PRAM imaging with digital resolution. **(C)** Zoom-in view of the AC + DC immunoassay on the PC surface (top) and the corresponding peak intensity value image (bottom). In this single-step assay, COVID-19 IgG (yellow) activates the system by specific binding to 2^{o}Ab-AuNPs or spike protein (light blue) on the PC surface, leading to capture of COVID-19 IgG-AuNPs and formation of sandwich immunocomplex on the PC. Peak intensity value image is obtained by PRAM allowing for the digital counting of particles for the quantitative analysis of COVID-19 IgG within 15 min. Images are not to scale. (For interpretation of the references to colour in this figure legend, the reader is referred to the Web version of this article.)

human serum in the clinically relevant concentration range.

3.2. Preparation and characterization of 2^{o}Ab-AuNPs conjugate

We prepared 2^{o}Ab-AuNPs by conjugating goat anti-human IgG Fc highly cross-adsorbed secondary antibodies with 80 nm diameter gold nanourchins via EDC/NHS chemistry and heterobifunctional polyethylene glycol (PEG) linkers. Gold nanourchins with a protruding tip morphology (Fig. S3A) were chosen as the label for PRAM-based imaging due to their enhanced light harvesting across the particle surface, and because their surface plasmon resonance wavelength closely matches the PC resonant reflection wavelength [38]. The as-prepared 2^{o}Ab-AuNPs were characterized by UV–Vis spectroscopy to confirm the conjugation of the secondary antibody (Fig. S3B). A slight red-shift (~5 nm) was observed after the antibody modification and the maximum absorption wavelength is approximately 625 nm, which perfectly matches the resonant reflection wavelength of the PC. As a gauge of conjugation performance, dynamic lighting scattering (DLS) measurements showed that 2^{o}Ab-AuNPs displayed an distinct increase of ~25.6 nm in average diameter compared to non-functionalized bare AuNPs (103.4 nm vs 77.8 nm, Fig. S3C).

3.3. Digital immunoassay for human COVID-19 IgG in buffer

As a proof-of-concept demonstration, we first tested the human COVID-19 IgG against SARS-Cov-2 spike protein in buffer using the developed single-step immunoassay. The PC coated with recombinant COVID-19 spike protein was first blocked with SuperBlock™ blocking buffer to eliminate non-specific binding during the assay. A series of human COVID-19 IgG samples in phosphate buffered saline (PBS) at

variable concentrations were simply mixed with 2°Ab-AuNPs, followed by the direct introduction into the polydimethylsiloxane (PDMS) container on the PC surface for PRAM imaging. As shown in Fig. 2A, the surface-attached AuNPs that form through the sandwich immunocomplexes were clearly observed at single-particle digital resolution after 30 min. The count of AuNPs increased with the increased human COVID-19 IgG concentration from 0 to 500 ng mL^{-1}. Fig. 2B show the counting of AuNPs using an optimized algorithm for PIV images. A customized watershed algorithm for the bound AuNPs is utilized to ensure the accuracy of the particle counting [25]. Fig. 2C presents the dose-response relationship obtained by correlating the AuNPs counts with COVID-19 IgG concentration. Detecting the target IgG in buffer, the PRAM-based single-step immunoassay has a wide dynamic range and good linear relationship from 0.1 ng mL^{-1} to 100 ng mL^{-1} (Fig. 2C and S4). The R square (R^2) is 0.986 (Table S1). The calculated LOD is determined by extrapolating the COVID-19 IgG concentration to a signal equal to a blank signal (all conditions the same, but no IgG present) plus 3 standard deviations (blank+3σ) [39], which is 62.3 ± 19.3 pg mL^{-1} for the assay in buffer. We also calculated the LOQ to be 565.2 ± 101.0 pg mL^{-1}, which is defined as the COVID-19 IgG concentration at a signal equal to a blank signal plus 10 standard deviations.

3.4. Selectivity of PRAM-based digital-resolution immunoassay

We next evaluated the selectivity of the method and its response to interfering proteins in human serum. Native human IgG and IgM were selected as control proteins due to their similarity to the target IgG and their abundance in serum [40]. We also tested human serum albumin (HSA) because it is the most abundant protein in human blood plasma [41]. As depicted in Fig. 3, all control proteins (10 ng mL^{-1}) show a small number of particles (HSA: 20 ± 3, IgM: 12 ± 2, IgG: 15 ± 4) and no significant difference to the blank control (18 ± 5) in PBS after 30 min. In contrast, the COVID-19 IgG at the same concentration results in an elevated number of AuNPs (144 ± 38) bound to the PC through specific antigen-antibody binding, which is 7 times higher than that of control proteins. We further examined complete human serum (100% human serum) which contains different types of interfering substances, including proteins, electrolytes, antigens and hormones. A small number of particles (34 ± 8) were observed, indicating that the 2°Ab-AuNPs can tolerate the complicated components in human serum. Taken together, the results demonstrate our PRAM-based immunoassay has good specificity towards human COVID-19 IgG and is not affected by a variety of protein interferences in human serum.

3.5. Digital detection of human COVID-19 IgG in serum samples

Having demonstrated AC + DC detection of human COVID-19 IgG in buffer with high sensitivity and selectivity, we next challenged the method with human serum samples spiked with human COVID-19 IgG. Interestingly, we found that the signal-to-noise ratio (SNR) of the assay relies on the volume mixing ratio of 2°Ab-AuNPs and serum samples. A relatively high SNR of 13.9 was achieved when 2°Ab-AuNPs and the human serum blank sample were mixed at a volume ratio of 6:4 compared to 5:5, which yielded a SNR of 5.1 (Fig. S5). Considering the natural IgG proteins in human serum may react with 2°Ab-AuNPs and therefore reduce the efficacy of the assay, we further increased the concentration of 2°Ab-AuNPs (2 × $[AuNPs]_0$, Abs_{625nm} = 0.155 ± 0.005) to obtain a SNR of 18.9 for the detection of 400 ng mL^{-1} COVID-19 IgG (Fig. S5). The AuNP counts were determined to be 643 ± 34. In contrast, for the same concentration of COVID-19 IgG in serum, 2°Ab-AuNPs with the original concentration (1 × $[AuNPs]_0$, Abs_{625nm} = 0.070 ± 0.005) only yielded an AuNP count of 132 ± 16. This number is much lower than that of assays performed in PBS for 100 ng mL^{-1} COVID-19 IgG (432 ± 111) using 1 × $[AuNPs]_0$. The optimal volume

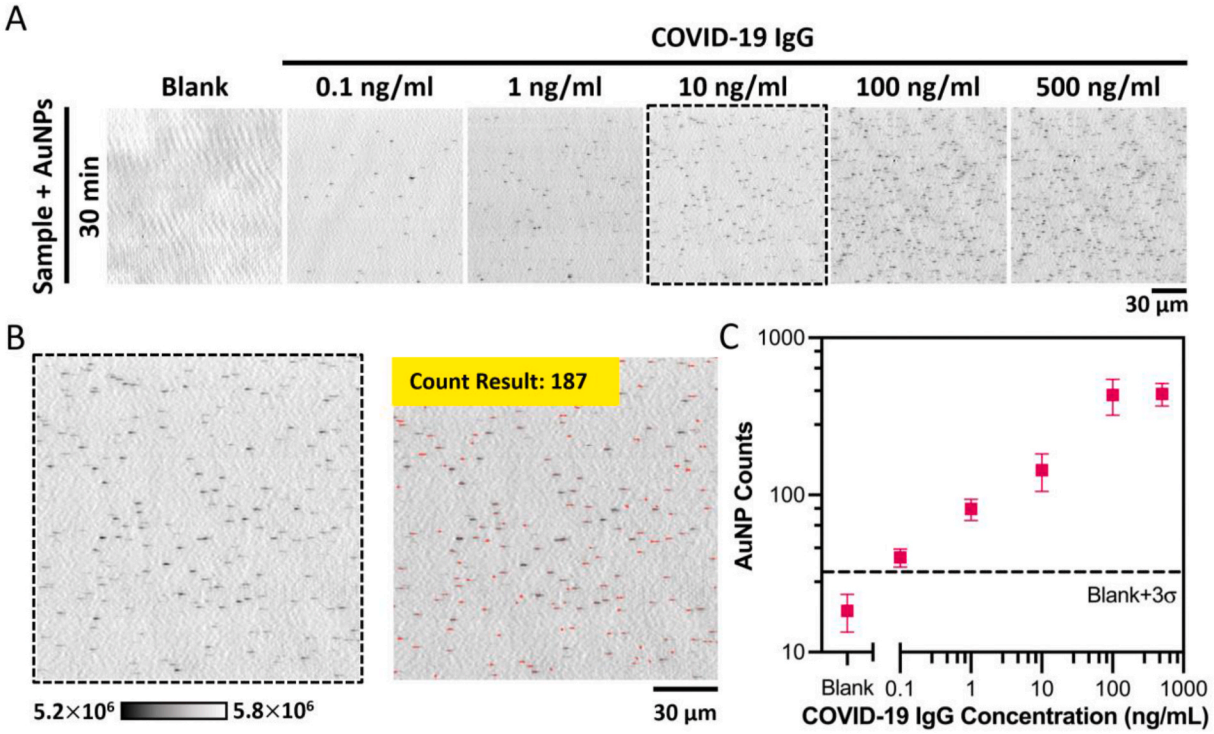

Fig. 2. Digital-resolution detection of human COVID-19 IgG by PRAM in buffer. (A) Peak intensity value PRAM images for different concentrations of COVID-19 IgG in PBS. Blank represents the negative control performed with no COVID-19 IgG in the test sample. The assay time was 30 min. **(B)** Left: expanded single tile from (A) (dashed tile). Right: digital counting of bound particles in the selected tile with a watershed algorithm. The detected individual particles are indicated by red dots. **(C)** Particle quantification as a function of COVID-19 IgG concentration in PBS at 30 min. The dashed horizontal line indicates the threshold (blank signal + 3 standard deviations). The error bars represent the standard deviation of three independent assays. (For interpretation of the references to colour in this figure legend, the reader is referred to the Web version of this article.)

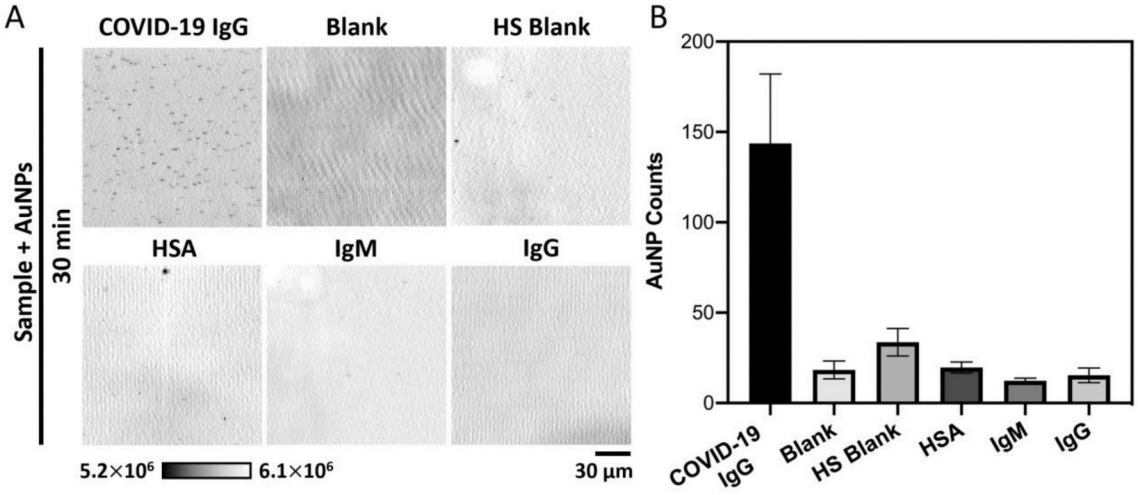

Fig. 3. Selectivity of PRAM-based digital-resolution immunoassay towards human COVID-19 IgG. (A) Peak intensity value images for COVID-19 IgG, control proteins (HSA, IgM and IgG) and blank controls. HS Blank represents COVID-19 IgG-free human serum control. The concentration of COVID-19 IgG, HSA, IgM and IgG is 10 ng mL^{-1}. The assay time was 30 min. **(B)** Quantification of particle count for comparison of COVID-19 and control experiments. The error bars represent the standard deviation of three independent assays.

mixing ratio of 6:4 and increased AuNP concentration (Abs_{625nm} = 0.155 ± 0.005) were used for the following experiments.

We tested a series of human COVID-19 IgG-spiked serum samples of 4 µL volume at concentrations of 0.1–500 ng mL^{-1}. COVID-19 IgG was diluted to the desired concentration in human serum and mixed with 2^{o}Ab-AuNPs for the PRAM-based immunoassay. As shown in Fig. 4A, the bound AuNPs were clearly observed in PIV images for all tested concentrations of COVID-19 IgG in human serum within 15 min. The counts of AuNPs decreased concomitantly with decreasing COVID-19 IgG concentration, and COVID-19 IgG can be differentiated from the blank control at concentration as low as 0.1 ng mL^{-1}. We incubated the assay for an additional 15 min, and repeated the imaging procedure to explore whether increased assay time would reduce the detection limit. Interestingly, the PIV images and quantitative analysis show that the AuNP counts after 30 min remain the same as those obtained after only 15 min (Fig. 4A and B). The results imply that the kinetics of antigen-antibody interaction in human serum are fast enough that assembly of the AuNP tagged immunocomplex is not limited by the rate of diffusion to the PC biosensor surface. As the 15 min sample incubation time is sufficient to obtain detection limits in the clinically relevant range, and the particle counts have reached a stable threshold, we conclude that the assay volume, sample size, and fluid compartment dimensions provide a robust environment for obtaining easily reproduced results. Fig. 4C depicts the dose response relationship between COVID-19 IgG concentration and counts of bound AuNPs on the PC. The calculated dynamic detection range is from 93.3 pg mL^{-1} to 25.7 ng mL^{-1}. The immunoassay has a good linear range from 0.1 to 100 ng mL^{-1} (Fig. S6). The R^2 is determined to be 0.995 and all the linear correlation coefficients are listed in Table S2. The calculated LOD and LOQ is 26.7 ± 7.7 pg mL^{-1} and 32.0 ± 8.9 pg mL-1, respectively. It is thus demonstrated that our PRAM-based single-step digital-resolution immunoassay is capable of quantitatively detecting serological antibody against SARS-CoV-2 with high sensitivity in 15 min.

It is noteworthy that the high sensitivity of our method rivals that of ELISA or CLIA which typically range 1–100 pg mL^{-1} [42]. It is > 50 times more sensitive than commercial pGOLD High Accuracy IgG/IgM Assay Kit (https://www.nirmidas.com/pgold-covid-19-igg-igm-assay-kit), which is based on NIR fluorescence and offers a detection limit of ~1.6 ng mL^{-1} for COVID-19 IgG [43]. In terms of assay time, our 15-min assay method is comparable to LIFA and substantially more rapid than ELISA and CLIA (>2 h). More importantly, with calibration against concentration standards, it can achieve quantitative detection of COVID-19 antibody which is vital for assessment of the level of immune response and identifying donors for blood transfusion therapy [12,44].

4. Conclusions

In summary, we have developed a single-step and washing-free immunoassay for rapid quantitative detection of serological human COVID-19 IgG with digital resolution, high sensitivity, low sample volume, and high selectivity. Taking advantage of the AC + DC assay principle, COVID-19 IgG proteins induce the activation of the functionalized AuNPs in solution and the specific binding of activated AuNPs to the PC, followed by the digital imaging by PRAM. We first demonstrated the proof-of-concept assay for highly sensitive and selective detection of human COVID-19 IgG in buffer and in human serum. We achieved a detection limit of 100 pg mL^{-1} with a 15 min assay time. Our method possesses many attractive features, such as easy operation, a simple assay cartridge, and the need of a small volume of serum sample (~4 µL).

Although the benchtop PRAM instrument was used in this work, we are developing portable and inexpensive instrument by utilizing LED illumination and a webcam-quality 2-dimensional image sensor that eliminates the spectrometer and requirement for line-scanning. We will describe the design and operation of the portable PRAM in a future publication as we consider how to perform serological assays in point of care settings. Given the broad set of assays that are performed using the sandwich assay approach used here, our method holds great promise for the development of a universal diagnostic platform for multiplexed detection of a variety of analytes, including antigens, proteins additional IgGs, cytokines, and other protein biomarkers.

Credit author statement

Bin Zhao, Methodology, Investigation, Data curation, Validation, Formal analysis, Writing – original draft. Congnyu Che, Investigation, Data curation, Validation, Formal analysis, Writing – original draft. Weijing Wang, Investigation, Data curation, Validation, Formal analysis, Writing – original draft. Nantao Li, Data curation, Formal analysis, Writing – review & editing. Brian T. Cunningham, Conceptualization, Funding acquisition, Writing – review & editing, Supervision.

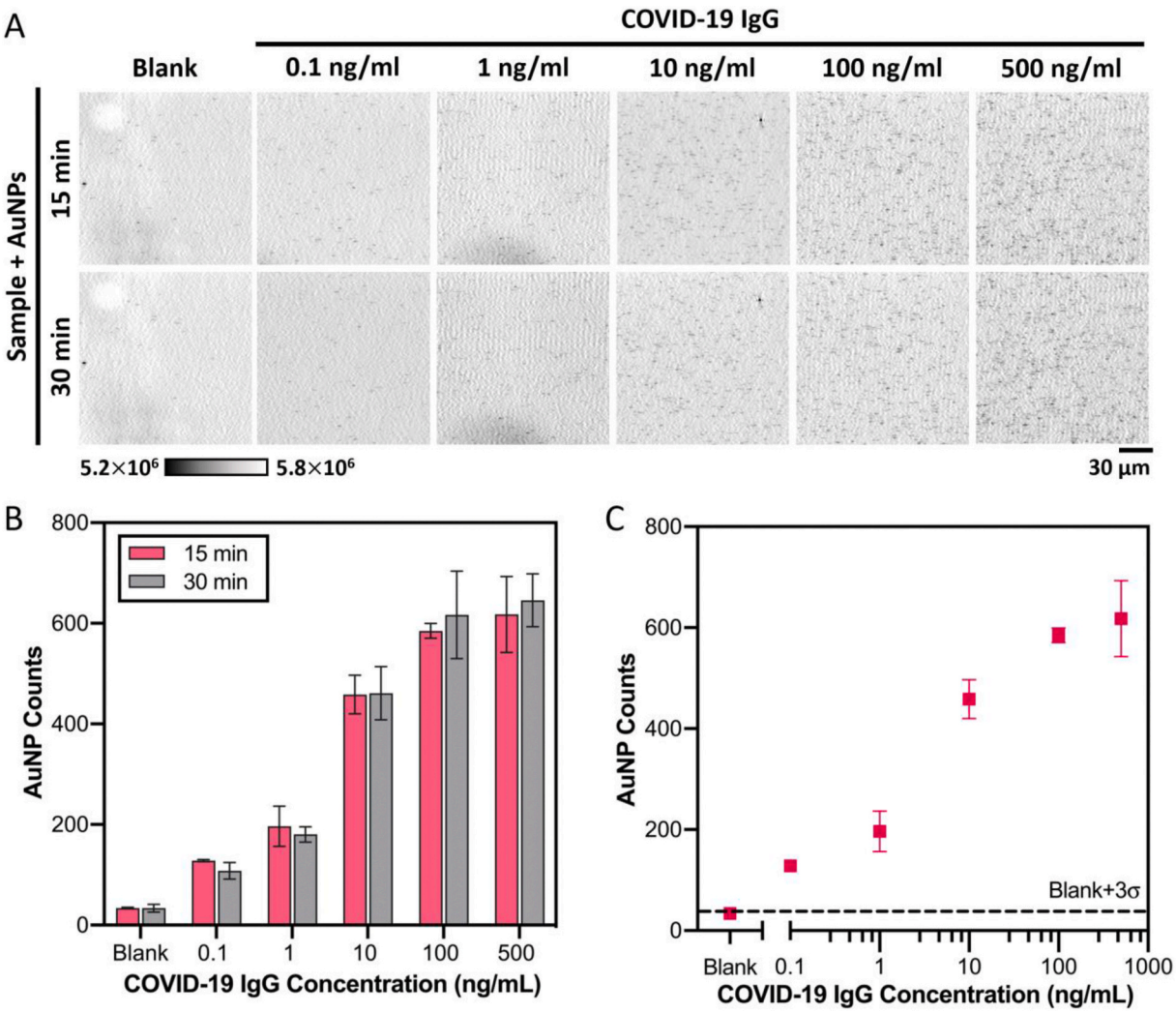

Fig. 4. AC + DC immunoassay of serological human COVID-19 IgG. (A) Peak intensity value images for human serum samples spiked with different concentrations of COVID-19 IgG. Images were obtained at 15 min and 30 min, respectively. Blank represents COVID-19 IgG-free (0 ng mL^{-1}) human serum control. **(B)** Quantitative analysis of particle count for variable concentration of COVID-19 IgG-spiked human serum samples at 15 min (pink) and 30 min (grey). **(C)** Quantification of AuNPs as a function of serological COVID-19 IgG concentration at 15 min. The dash line represents for the threshold (blank signal + 3 standard deviations). The error bars in (B) and (C) represent the standard deviation of three independent assays. (For interpretation of the references to colour in this figure legend, the reader is referred to the Web version of this article.)

Declaration of competing interest

The authors declare that they have no known competing financial interests or personal relationships that could have appeared to influence the work reported in this paper.

Acknowledgements

This work is supported by the National Institutes of Health (NIH) R21 AI130562 and R01 AI20683. B. Z. is supported by a Carl R. Woese Institute for Genomic Biology (IGB) fellowship in the Center for Genomic Diagnostics. The authors gratefully acknowledge the members of the Nanosensors Group (NSG) and staff in the Nick Holonyak Jr. Micro and Nanotechnology Laboratory for their support.

Appendix A. Supplementary data

Supplementary data to this article can be found online at https://doi.org/10.1016/j.talanta.2020.122004.

References

[1] P. Zhou, X.-L. Yang, X.-G. Wang, B. Hu, L. Zhang, W. Zhang, H.-R. Si, Y. Zhu, B. Li, C.-L. Huang, H.-D. Chen, J. Chen, Y. Luo, H. Guo, R.-D. Jiang, M.-Q. Liu, Y. Chen, X.-R. Shen, X. Wang, X.-S. Zheng, K. Zhao, Q.-J. Chen, F. Deng, L.-L. Liu, B. Yan, F.-X. Zhan, Y.-Y. Wang, G.-F. Xiao, Z.-L. Shi, A pneumonia outbreak associated with a new coronavirus of probable bat origin, Nature 579 (7798) (2020) 270–273.

[2] W. Wang, Y. Xu, R. Gao, R. Lu, K. Han, G. Wu, W. Tan, Detection of SARS-CoV-2 in different types of clinical specimens, J. Am. Med. Assoc. 323 (18) (2020) 1843–1844.

[3] J.F.-W. Chan, C.C.-Y. Yip, K.K.-W. To, T.H.-C. Tang, S.C.-Y. Wong, K.-H. Leung, A. Y.-F. Fung, A.C.-K. Ng, Z. Zou, H.-W. Tsoi, G.K.-Y. Choi, A.R. Tam, V.C.-C. Cheng, K.-H. Chan, O.T.-Y. Tsang, K.-Y. Yuen, Improved molecular diagnosis of COVID-19 by the novel, highly sensitive and specific COVID-19-RdRp/hel real-time reverse transcription-PCR assay validated in vitro and with clinical specimens, J. Clin. Microbiol. 58 (5) (2020) e00310–e00320.

[4] B. Udugama, P. Kadhiresan, H.N. Kozlowski, A. Malekjahani, M. Osborne, V.Y. C. Li, H. Chen, S. Mubareka, J.B. Gubbay, W.C.W. Chan, Diagnosing COVID-19: the Disease and tools for detection, ACS Nano 14 (4) (2020) 3822–3835.

[5] Z. Li, Y. Yi, X. Luo, N. Xiong, Y. Liu, S. Li, R. Sun, Y. Wang, B. Hu, W. Chen, Y. Zhang, J. Wang, B. Huang, Y. Lin, J. Yang, W. Cai, X. Wang, J. Cheng, Z. Chen, K. Sun, W. Pan, Z. Zhan, L. Chen, F. Ye, Development and clinical application of a rapid IgM-IgG combined antibody test for SARS-CoV-2 infection diagnosis, J. Med. Virol. 92 (9) (2020) 1518–1524.

[6] I.M. Mackay, K.E. Arden, A. Nitsche, Real-time PCR in virology, Nucleic Acids Res. 30 (6) (2002) 1292–1305.

[7] S.L. Emery, D.D. Erdman, M.D. Bowen, B.R. Newton, J.M. Winchell, R.F. Meyer, S. Tong, B.T. Cook, B.P. Holloway, K.A. McCaustland, P.A. Rota, B. Bankamp, L. E. Lowe, T.G. Ksiazek, W.J. Bellini, L.J. Anderson, Real-time reverse transcription-polymerase chain reaction assay for SARS-associated coronavirus, Emerg. Infect. Dis. 10 (2) (2004) 311–316.
[8] L.J. Carter, L.V. Garner, J.W. Smoot, Y. Li, Q. Zhou, C.J. Saveson, J.M. Sasso, A. C. Gregg, D.J. Soares, T.R. Beskid, S.R. Jervey, C. Liu, Assay techniques and test development for COVID-19 diagnosis, ACS Cent. Sci. 6 (5) (2020) 591–605.
[9] Q.-X. Long, B.-Z. Liu, H.-J. Deng, G.-C. Wu, K. Deng, Y.-K. Chen, P. Liao, J.-F. Qiu, Y. Lin, X.-F. Cai, D.-Q. Wang, Y. Hu, J.-H. Ren, N. Tang, Y.-Y. Xu, L.-H. Yu, Z. Mo, F. Gong, X.-L. Zhang, W.-G. Tian, L. Hu, X.-X. Zhang, J.-L. Xiang, H.-X. Du, H.-W. Liu, C.-H. Lang, X.-H. Luo, S.-B. Wu, X.-P. Cui, Z. Zhou, M.-M. Zhu, J. Wang, C.-J. Xue, X.-F. Li, L. Wang, Z.-J. Li, K. Wang, C.-C. Niu, Q.-J. Yang, X.-J. Tang, Y. Zhang, X.-M. Liu, J.-J. Li, D.-C. Zhang, F. Zhang, P. Liu, J. Yuan, Q. Li, J.-L. Hu, J. Chen, A.-L. Huang, Antibody responses to SARS-CoV-2 in patients with COVID-19, Nat. Med. 26 (6) (2020) 845–848.
[10] C. Dobaño, M. Vidal, R. Santano, A. Jiménez, J. Chi, D. Barrios, G. Ruiz-Olalla, N. R. Melero, C. Carolis, D. Parras, P. Serra, P.M. de Aguirre, F. Carmona-Torre, G. Reina, P. Santamaria, A. Mayor, A. García-Basteiro, L. Izquierdo, R. Aguilar, G. Moncunill, Highly sensitive and specific multiplex antibody assays to quantify immunoglobulins M, A and G against SARS-CoV-2 antigens, bioRxiv (2020) 2020, 06.11.147363.
[11] M.Z. Tay, C.M. Poh, L. Rénia, P.A. MacAry, L.F.P. Ng, The trinity of COVID-19: immunity, inflammation and intervention, Nat. Rev. Immunol. 20 (6) (2020) 363–374.
[12] K. Duan, B. Liu, C. Li, H. Zhang, T. Yu, J. Qu, M. Zhou, L. Chen, S. Meng, Y. Hu, C. Peng, M. Yuan, J. Huang, Z. Wang, J. Yu, X. Gao, D. Wang, X. Yu, L. Li, J. Zhang, X. Wu, B. Li, Y. Xu, W. Chen, Y. Peng, Y. Hu, L. Lin, X. Liu, S. Huang, Z. Zhou, L. Zhang, Y. Wang, Z. Zhang, K. Deng, Z. Xia, Q. Gong, W. Zhang, X. Zheng, Y. Liu, H. Yang, D. Zhou, D. Yu, J. Hou, Z. Shi, S. Chen, Z. Chen, X. Zhang, X. Yang, Effectiveness of convalescent plasma therapy in severe COVID-19 patients, Proc. Natl. Acad. Sci. U. S. A. 117 (17) (2020) 9490–9496.
[13] W. Liu, L. Liu, G. Kou, Y. Zheng, Y. Ding, W. Ni, Q. Wang, L. Tan, W. Wu, S. Tang, Z. Xiong, S. Zheng, Evaluation of nucleocapsid and spike protein-based enzyme-linked immunosorbent assays for detecting antibodies against SARS-CoV-2, J. Clin. Microbiol. 58 (6) (2020) e00461, 20.
[14] K.G. Beavis, S.M. Matushek, A.P.F. Abeleda, C. Bethel, C. Hunt, S. Gillen, A. Moran, V. Tesic, Evaluation of the EUROIMMUN anti-SARS-CoV-2 ELISA assay for detection of IgA and IgG antibodies, J. Clin. Virol. 129 (2020) 104468, 104468.
[15] F. Amanat, D. Stadlbauer, S. Strohmeier, T.H.O. Nguyen, V. Chromikova, M. McMahon, K. Jiang, G.A. Arunkumar, D. Jurczyszak, J. Polanco, M. Bermudez-Gonzalez, G. Kleiner, T. Aydillo, L. Miorin, D.S. Fierer, L.A. Lugo, E.M. Kojic, J. Stoever, S.T.H. Liu, C. Cunningham-Rundles, P.L. Felgner, T. Moran, A. García-Sastre, D. Caplivski, A.C. Cheng, K. Kedzierska, O. Vapalahti, J.M. Hepojoki, V. Simon, F. Krammer, A serological assay to detect SARS-CoV-2 seroconversion in humans, Nat. Med. 26 (2020) 1033–1036.
[16] L. Cinquanta, D.E. Fontana, N. Bizzaro, Chemiluminescent immunoassay technology: what does it change in autoantibody detection? Autoimmun. Highlights 8 (1) (2017) 9.
[17] Y. Wan, Z. Li, K. Wang, T. Li, P. Liao, Performance verification of detecting COVID-19 specific antibody by using four chemiluminescence immunoassay systems, medRxiv (2020) 2020, 04.27.20074849.
[18] G.A. Posthuma-Trumpie, J. Korf, A. van Amerongen, Lateral flow (immuno)assay: its strengths, weaknesses, opportunities and threats. A literature survey, Anal. Bioanal. Chem. 393 (2) (2009) 569–582.
[19] K.J. Paiva, R.D. Grisson, P.A. Chan, J.R. Lonks, E. King, R.C. Huard, D.L. Pytel-Parenteau, G.H. Nam, E. Yakirevich, S. Lu, Validation and performance comparison of three SARS-CoV-2 antibody assays, bioRxiv (2020) 2020, 05.29.124776.
[20] C. Sheridan, Fast, portable tests come online to curb coronavirus pandemic, Nat. Biotechnol. 38 (5) (2020) 515–518.
[21] T. Suo, X. Liu, J. Feng, M. Guo, W. Hu, D. Guo, H. Ullah, Y. Yang, Q. Zhang, X. Wang, M. Sajid, Z. Huang, L. Deng, T. Chen, F. Liu, K. Xu, Y. Liu, Q. Zhang, Y. Liu, Y. Xiong, G. Chen, K. Lan, Y. Chen, ddPCR: a more accurate tool for SARS-CoV-2 detection in low viral load specimens, Emerg. Microb. Infect. 9 (1) (2020) 1259–1268.
[22] J. Cao, H.-L. Liu, J.-M. Yang, Z.-Q. Li, D.-R. Yang, L.-N. Ji, K. Wang, X.-H. Xia, SERS detection of nucleobases in single silver plasmonic nanopores, ACS Sens. 5 (7) (2020) 2198–2204.
[23] M. Piliarik, V. Sandoghdar, Direct optical sensing of single unlabelled proteins and super-resolution imaging of their binding sites, Nat. Commun. 5 (1) (2014) 4495.
[24] H. Inan, M. Poyraz, F. Inci, M.A. Lifson, M. Baday, B.T. Cunningham, U. Demirci, Photonic crystals: emerging biosensors and their promise for point-of-care applications, Chem. Soc. Rev. 46 (2) (2017) 366–388.
[25] T.D. Canady, N. Li, L.D. Smith, Y. Lu, M. Kohli, A.M. Smith, B.T. Cunningham, Digital-resolution detection of microRNA with single-base selectivity by photonic resonator absorption microscopy, Proc. Natl. Acad. Sci. U. S. A. 116 (39) (2019) 19362–19367.
[26] Y. Zhuo, J.S. Choi, T. Marin, H. Yu, B.A. Harley, B.T. Cunningham, Quantitative analysis of focal adhesion dynamics using photonic resonator outcoupler microscopy (PROM), Light: Sci. Appl. 7 (1) (2018) 9.
[27] V. Konopsky, T. Mitko, K. Aldarov, E. Alieva, D. Basmanov, A. Moskalets, A. Matveeva, O. Morozova, D. Klinov, Photonic crystal surface mode imaging for multiplexed and high-throughput label-free biosensing, Biosens. Bioelectron. 168 (2020) 112575.
[28] A.S. Rizvi, G. Murtaza, D. Yan, M. Irfan, M. Xue, Z.H. Meng, F. Qu, Development of molecularly imprinted 2D photonic crystal hydrogel sensor for detection of L-kynurenine in human serum, Talanta 208 (2020) 120403.
[29] C. Chen, Z.-Q. Dong, J.-H. Shen, H.-W. Chen, Y.-H. Zhu, Z.-G. Zhu, 2D photonic crystal hydrogel sensor for tear glucose monitoring, ACS Omega 3 (3) (2018) 3211–3217.
[30] H. Zhang, J. Lv, Z. Jia, Efficient fluorescence resonance energy transfer between quantum dots and gold nanoparticles based on porous silicon photonic crystal for DNA detection, Sensors 17 (5) (2017) 1078.
[31] C. Che, N. Li, K.D. Long, M.Á. Aguirre, T.D. Canady, Q. Huang, U. Demirci, B. T. Cunningham, Activate capture and digital counting (AC+ DC) assay for protein biomarker detection integrated with a self-powered microfluidic cartridge, Lab Chip 19 (23) (2019) 3943–3953.
[32] D. Vilela, A. Romeo, S. Sánchez, Flexible sensors for biomedical technology, Lab Chip 16 (3) (2016) 402–408.
[33] K.D. Long, E.V. Woodburn, H.M. Le, U.K. Shah, S.S. Lumetta, B.T. Cunningham, Multimode smartphone biosensing: the transmission, reflection, and intensity spectral (TRI)-analyzer, Lab Chip 17 (19) (2017) 3246–3257.
[34] Q. Huang, N. Li, H. Zhang, C. Che, F. Sun, Y. Xiong, T.D. Canady, B.T. Cunningham, Critical Review: digital resolution biomolecular sensing for diagnostics and life science research, Lab Chip 20 (16) (2020) 2816–2840.
[35] Z. Li, B. Zhao, D. Wang, Y. Wen, G. Liu, H. Dong, S. Song, C. Fan, DNA nanostructure-based universal microarray platform for high-efficiency multiplex bioanalysis in biofluids, ACS Appl. Mater. Interfaces 6 (20) (2014) 17944–17953.
[36] B. Zhao, J. Shen, S. Chen, D. Wang, F. Li, S. Mathur, S. Song, C. Fan, Gold nanostructures encoded by non-fluorescent small molecules in polyA-mediated nanogaps as universal SERS nanotags for recognizing various bioactive molecules, Chem. Sci. 5 (11) (2014) 4460–4466.
[37] Q. Huang, B.T. Cunningham, Microcavity-Mediated spectrally tunable amplification of absorption in plasmonic nanoantennas, Nano Lett. 19 (8) (2019) 5297–5303.
[38] F. Hao, C.L. Nehl, J.H. Hafner, P. Nordlander, Plasmon resonances of a gold nanostar, Nano Lett. 7 (3) (2007) 729–732.
[39] D.M. Rissin, C.W. Kan, T.G. Campbell, S.C. Howes, D.R. Fournier, L. Song, T. Piech, P.P. Patel, L. Chang, A.J. Rivnak, E.P. Ferrell, J.D. Randall, G.K. Provuncher, D. R. Walt, D.C. Duffy, Single-molecule enzyme-linked immunosorbent assay detects serum proteins at subfemtomolar concentrations, Nat. Biotechnol. 28 (6) (2010) 595–599.
[40] A. Gonzalez-Quintela, R. Alende, F. Gude, J. Campos, J. Rey, L.M. Meijide, C. Fernandez-Merino, C. Vidal, Serum levels of immunoglobulins (IgG, IgA, IgM) in a general adult population and their relationship with alcohol consumption, smoking and common metabolic abnormalities, Clin. Exp. Immunol. 151 (1) (2008) 42–50.
[41] G. Fanali, A. di Masi, V. Trezza, M. Marino, M. Fasano, P. Ascenzi, Human serum albumin: from bench to bedside, Mol. Aspect. Med. 33 (3) (2012) 209–290.
[42] S. Zhang, A. Garcia-D'Angeli, J.P. Brennan, Q. Huo, Predicting detection limits of enzyme-linked immunosorbent assay (ELISA) and bioanalytical techniques in general, Analyst 139 (2) (2014) 439–445.
[43] B. Zhang, B.A. Pinsky, J.S. Ananta, S. Zhao, S. Arulkumar, H. Wan, M.K. Sahoo, J. Abeynayake, J.J. Waggoner, C. Hopes, M. Tang, H. Dai, Diagnosis of Zika virus infection on a nanotechnology platform, Nat. Med. 23 (5) (2017) 548–550.
[44] L. Zhang, R. Pang, X. Xue, J. Bao, S. Ye, Y. Dai, Y. Zheng, Q. Fu, Z. Hu, Y. Yi, Anti-SARS-CoV-2 virus antibody levels in convalescent plasma of six donors who have recovered from COVID-19, Aging (Albany NY) 12 (8) (2020) 6536–6542.